JCARME
ISSN: 2228-7922
Journal of Computational and Applied Research in Mechanical Engineering
Vol. 8, No. 1, pp. 1-14
jcarme.sru.ac.ir

Favorable plug shape of an aerospike nozzle in design, over and under expansion conditions

A. Shahrokhi[a] and S. Noori[b,*]

[a]*School of Creative Arts and Engineering, Staffordshire University, ST42DE, UK*
[b]*Aerospace Department, Amirkabir University of Technology,Tehran, Iran*

Article info:
Received: 23/04/2017
Accepted: 25/12/2017
Online: 10/04/2018

Keywords:
Aerospike nozzle,
Cubic B-Spline,
Turbulence,
Plug shape.

Abstract
The influence of plug shape on the performance of an aerospike nozzle thrust force is studied in different back pressure conditions. To generate smooth plug contours, Cubic B-Spline technique is employed. In the current research, basis functions are obtained using Deboor's relation. The flow field around the aerospike nozzle is investigated implementing various shapes, and the best of the generated configurations is determined. The flow field is simulated using Navier-Stokes equations and k-ε turbulence model. A triangle unstructured grid is applied for discretization of the governing equations. The computational methodology utilizes steady state density-based formulation, and a finite volume cell centered scheme is used to discretize the flow field equations. The flow field is divided into several zones to accelerate the solution convergence,, and an appropriate initial condition is assigned to each zone. Six different shapes of the plug are generated, and the effect of the spike shape on the formation of the shock and expansion waves is investigated in each case. The thrust force is calculated for each case, and the best configuration is determined in terms of the maximum thrust generation. Eventually, the temperature distribution is calculated along the nozzle for further investigations, and it is concluded that the best configurations show a lower temperature rise compared to other designs.

Nomenclature

x, y	Cartesian coordinates of the surface	u_i	Non-decreasing set of real numbers (knot sequence)
$N_{i,k}$	i*th* B-spline basis function of order k	P_{atm}	Atmospheric Pressure
u	Independent B-spline variable	P_{design}	Design Pressure
(X_i, Y_i)	B-spline control points		

1. Introduction

To achieve relatively better performance than Conventional bell nozzles, the aerospike engine has been vastly studied from early 60th. These kinds of nozzles possess the best capabilities for continuous altitude compensation. The aerospike rocket engine consists of a rocket thruster, cowl,

*Corresponding author
Email address: s_noori@aut.ac.ir

aerospike nozzle, and plug base region (Fig. 1). In theory, the optimal thrust for a given jet or rocket engine occurs when the nozzle exit pressure equals surrounding pressure. Considering other design variables fixed, there exists only one area ratio of exit area to throat area at a given altitude for optimal expansion in conventional nozzles. However, the plug contour allows the exit flow to adjust to the ambient pressure through changing the flow-field structure during the flight from low to high altitudes [1]. Therefore, compared to the conventional bell nozzles, unbounded expansion of the jet provides better performance over the entire flight. In addition, an appropriate design of truncated spike can decrease the engine size and weight with minimal performance losses [2,3].

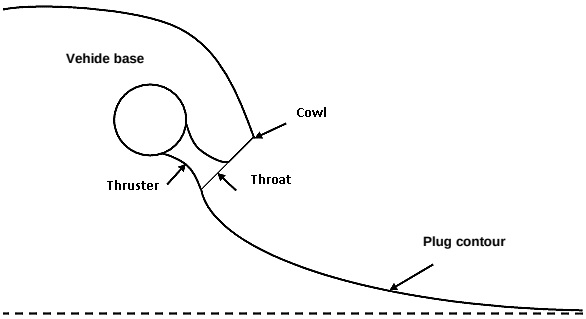

Fig. 1. Aerospike nozzle components.

Since the external flow pattern plays a vital rule in the performance of aerospike nozzles, several researches focused on the flow phenomena that can improve the efficiency of the entire propulsion system and the choice of an appropriate design which can develop such flows. Besnard et al. [4] applied the axisymmetric aerospike nozzle in a propulsion system of sounding rockets and demonstrated a considerable gain in the rockets' performance.

A technique which can remarkably enhance the maximum thrust generation of an aerospike nozzle is the use of dual expander cycles. The utilization of this design can practically maximize the efficiency of the nozzle [1]. Mcvay [5] studied the dual-expander aerospike nozzle upper stage rocket engine design methodology to improve the engine performance by increasing specific impulse and thrust-to-weight ratio while maintaining similar or better thrust levels than other engine concepts.In order to study the aerospike flow, several experiments have been designed and developed. A number of tests have been built up for the utilization of hybrid rocket motors on aerospike nozzles [6, 7]. Niimi et al. [8] investigated the flow field visualization around the linear aerospike nozzle in the wide range of pressure ratios.

One of the problems with the aerospike nozzles is the high-temperature flow over the plug. Wang [9] conducted computational heat transfer analyses to study the effect of the fence on the base heating of an X-33 aerospike engine. Around a decade later, Zebbiche and Youbi [10] investigated the supersonic two-dimensional plug nozzle at high temperatures. The goal of their research was to consider the dissociation of the gas molecules. Verma [11] studied the influence of annular conical spike nozzle and compared the performance of this nozzle with conical plug.

Recently, the behavior of the aerospike flow is numerically simulated, and a number of geometries are investigated. A problem with aerospike nozzles, which practically limits their applications in a rocket propulsion system, is their weight. A popular way to minimize this problem is to truncate plug-base in length. Larger amounts of base truncation lead to thrust loss particularly in over-expansion conditions though. To deal with this problem, a technique, called base bleed, is used, in which a secondary flow is injected at the base of the truncated plug. Naghib-Lahouti and Tolouei [12] studied the effect of the base-bleed on thrust force of aerospike nozzle, and an optimum amount of base bleed in different working conditions is offered. Zilic et al. [13] numerically examined thrust performance of the linear aerospike nozzle micro-thruster for various nozzle spike lengths and flow parameters in order to identify optimal geometry and operating conditions.

Plug shape remarkably influences the external flow and so the performance of the aerospike propulsion. The optimization of spike shape was considered by Simpson and Mistree [14] using Kriging method and response surface modeling. The optimal contouring of the two-dimensional and axisymmetric spike nozzles was studied by Kraiko and Tillyayeva [15]. The method can obtain the maximum thrust for given dimensions and external pressure. A numerical investigation of external air slipstream effects on the flow

properties and thrust performance of the plug nozzle was presented by Bozic and Porrmann [16]. Due to their unique characteristics and high adaptability to altitude changes, the aerospike nozzles are excellent candidates for orbit launching vehicles [17].

Accordingly, the main characteristic of the aerospike nozzles is the ability to compensate for the thrust changes with altitude. This priority is provided by the plug contour which allows the flow expansion to continue outside the convergent nozzle. Hence, as pointed out, the shape of the plug can highly influence the performance of the aerospike nozzle. Consequently as mentioned previously, the appropriate shape which possesses the maximum thrust in all conditions is a challenging subject.

The focus of this research is to generate a plug contour which can produce a favorable thrust force in design, over and under expansion conditions. Following this purpose, different plug shapes are generated using the B-Spline method and the flow field is solved around each nozzle. The thrust forces are then determined, and the best shape is identified among the generated shapes.

2. Flow characteristics of an aerospike nozzle

As the flow exits the nozzle throat, expansion waves occur over the lip cowl and along the plug. The exit flow forms a free boundary at the lip cowl which extends towards the ambient atmosphere. As the altitude is varied, different flow patterns happen along the aerospike nozzle. In theory, the optimal thrust for a given jet or rocket engine occurs when the nozzle exit pressure equals the surrounding pressure. In the design or optimum condition, the expansion waves end at the trailing part of the plug, and the free boundary is parallel to the plug axis.

When the nozzle is exposed to high ambient pressure, e.g., low amplitudes, the free boundary flow is pushed towards the nozzle walls. As a direct consequence of this, the compression waves reflect onto the central part of the nozzle. The waves impacting the plug increase pressure on the surface, thereby increasing the plug component of thrust. The expansion waves terminate before the end of the plug. This condition is called over-expansion.

As the vehicle ascends to high altitudes, the ambient pressure decreases and the free boundary expands considerably and further away from the plug contour. The free boundary diverges outward from the plug center. In this case, the compression waves move downstream and eventually cease to impact on the plug. The pressure profile on the plug contour becomes constant and no longer varies with ambient pressure. This condition is called under-expansion.

In addition to the inherent loss of thrust, the conventional nozzle might suffer from problems including shock waves and flow separation in the divergent section, thrust oscillation, and flow asymmetry in over-expansion conditions. Compared to the conventional bell nozzles, unbounded expansion of the jet provides overlay better performance in aerospike nozzles. Design, under-expansion and over-expansion conditions of an aerospike nozzle are illustrated in Fig. 2.

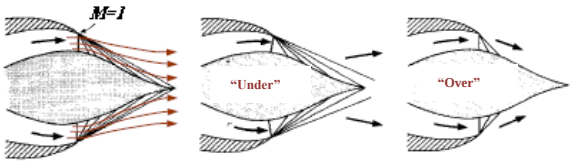

Fig. 2. Flow properties in design, under- and over-expansion conditions.

3. Geometry of the plug

The B-Spline method for curve representation is then implemented for the generation of different plug contours. This method is illustrated as follows:

3.1. Generation of the plug shapes

One of the key points about the aerospike nozzle is the selection of a suitable shape that can provide the maximum thrust force in different flow conditions which inevitably occur throughout the flight. There are several methods like the method of characteristics and the approximate method which can generate a suitable shape for design condition with no shock waves over the spike. However, the generated shape may not be efficient in other flight conditions. Consequently, utilization of a suitable shape which maintains its efficiency in a wide range of altitudes is of special

importance. One of the most popular methods for curve representation which is used in this research is B-Spline. This method introduces control points around the geometry. These points are then used to define the arbitrary shape. Several researchers employed B-Spline approach to parameterize the aerodynamic shapes during the optimization process [10]. The B-Spline method defines arbitrary shapes using a number of control points around the geometry. This method for defining the shape possesses acceptable flexibility in generating spikes with different curvature and inclinations while offering smooth curves.

In a B-spline representation, the x and y coordinates of the surfaces are written in a parametric form.

$$x(u)=\sum_{i=1}^{n+1} X_i N_{i,k}(u) \qquad n \geq k-1 \qquad (1)$$
$$y(u)=\sum_{i=1}^{n+1} Y_i N_{i,k}(u)$$

Therefore, The B-spline basis functions of an arbitrary dimension *n* can be evaluated as linear combinations of basis functions of a degree lower. The B-spline basis functions are obtained using De boor's relation:

$$N_{i,k}(u)=\frac{u-u_i}{u_{i+k-1}-u_i} N_{i,k-1}(u) + \frac{u_{i+k}-u}{u_{i+k}-u_{i+1}} N_{i+1,k-1}(u) \qquad (2)$$

where

$$N_{i,1}(u)=\begin{cases}1, & u_i < u < u_{i+1}\\ 0, & otherwise\end{cases} \qquad (3)$$

The number of knots is equal to the dimension of the basis function plus the order of the B-spline curve. Since basis functions are based on knot differences, the shape of the basis functions is only dependent on the knot spacing and not specific knot values. Comparing with other polynomials, the B-spline curves have the advantage of limiting the dimension of the polynomial to a user-defined level without changing the number of control points. The B-Spline of order 3 is used in this research together with 16 control points. The first and the last control points are fixed, and the B-Spline curves are fixed to these points. The six different shapes generated using cubic B-Spline method are illustrated in Fig. 3. The shapes are generated with different curvatures especially at the first half of the plug.

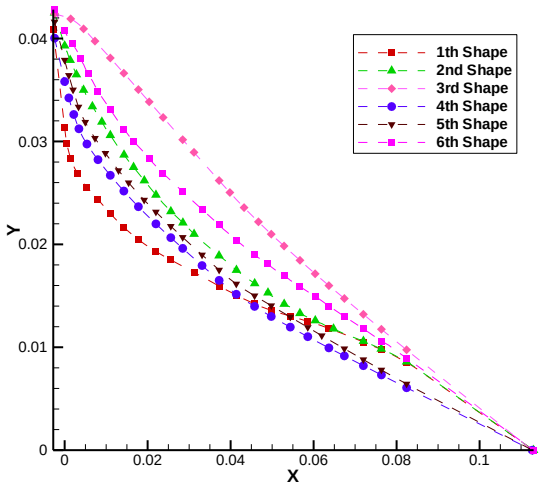

Fig. 3. Spike shapes generated using cubic B-Spline.

4. Numerical analysis of the flow

The numerical analysis of the internal and external flow of the aerospike nozzle is performed using Navier-Stokes equations considering turbulent effects. The computational technique utilizes steady state density-based Navier-Stokes equations. The numerical discretization of the flow field equations is based on a finite volume cell centered scheme. The viscous terms are evaluated by central differencing, and the eddy viscosity is modeled utilizing the standard k-ε method. The flow is assumed to be axisymmetric around the aerospike axis although three-dimensional equations are used for this study.

To increase grid spacing efficiency, the flow field is divided into several zones. Each zone is facilitated with proper unstructured triangle grid. Besides appropriate initial conditions is offered for each zone to accelerate the solution convergence. Fig. 4 demonstrates the zones and their corresponding grid distribution in the flow field. The solution convergence is remarkably increased through controlling the grid density. and providing appropriate initial conditions in each zone.

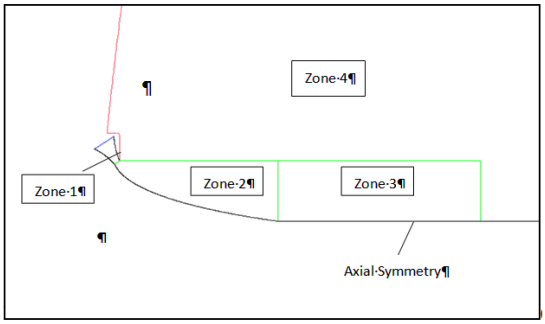

Fig. 4. Flow field division.

Flow field grid spacing is shown in Fig. 5 in the vicinity of the plug center. The grid density increases towards the throat and the remaining computational domain coarseness increases outward the nozzle outlet. The grid independency is checked for each configuration using different resolutions, and an appropriate grid is selected.

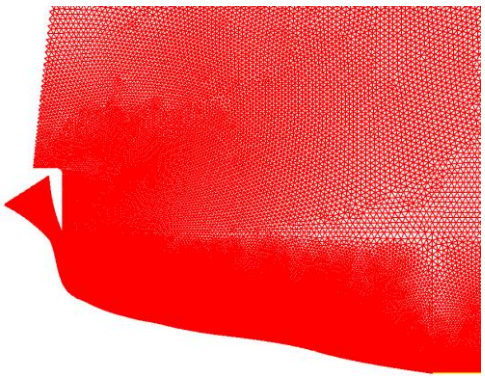

Fig. 5. Grid spacing in the vicinity of the plug.

The number of the cells is apparently different in each shape, but the number of approximately 150000 cells is used. Average properties of the combustion products resulting from chemical reaction of ethanol and oxygen have been assumed for the fluids in all regions. These properties satisfy the following relation:

$$C_p = \frac{\gamma R}{M(\gamma - 1)} \tag{4}$$

where

γ =1.21
C_P =1286.68 J/kgK
M =37.23 g/mol.

In this work, the convergence is confirmed considering two criteria. One of them is the reduction of the global residual of the solution of all governing equations to the order of 10^{-5}. The other criterion is the establishment of mass balance among inlet, far-field and outlet boundaries. In all shapes, the solution process is continued until both criteria are satisfied. One of the most suitable criteria for the measurement of the performance of an aerospike nozzle is the thrust of the propulsion system. For an axisymmetric aerospike nozzle, thrust is calculated using the following relation:

$$F = \int(\rho V dA)V_x + \int(P - P_{atm})\,\mathrm{Cos}\theta_t dA + \int(P - P_{atm})\mathrm{Sin}\theta_t dA \tag{5}$$

The first two terms are integrated on the throat of the convergent section, while the third term is integrated on the entire plug surface.

5. Results and discussion

This section describes numerical modeling and analysis of the internal and external flow of different aerospike nozzle shapes introduced in previous sections. The flow properties are computed for the aerospike nozzles considering six spike shapes introduced in Fig. 3. The objective of the analysis is to compare the thrust force of different spike shapes to decide on the most suitable shape for the plug. The comparison is made in the design ($P_{atm}/P_{design} = 1.0$), over ($P_{atm}/P_{design} = 4.0$) and under expansion ($P_{atm}/P_{design} = 0.41$) conditions. Pressure ratios are shown as PR during the rest of this paper.

5.1. Design condition

The method presented in this research is verified with the results of an aerospike nozzle of the 4-5 KN thrust class in design condition with the specifications originally introduced in [4]. The condition implied at the inlet of the convergent section is specific mass flow of 3.25757 kg/s, total temperature of 1577.826 K and pressure of 2045430 N/m^2. The geometrical parameters and the exit Mach number obtained through using the

approximate method mentioned above are listed in Table 1. The Mach number and pressure contours of shape 1 are shown in Figs. 6 and 7, respectively. It can be seen that a strong shock occurs downstream of the convergent part of the nozzle. Weak expansion waves are formed downstream near the end of the plug.

Table1. Aerospike nozzle specifications.

Item	Parameter	Value
1	Throat angle	57.1665°
2	Throat radius	0.04522(m)
3	Exhaust Mach number	2.80434
4	Exhaust radius	0.04788(m)

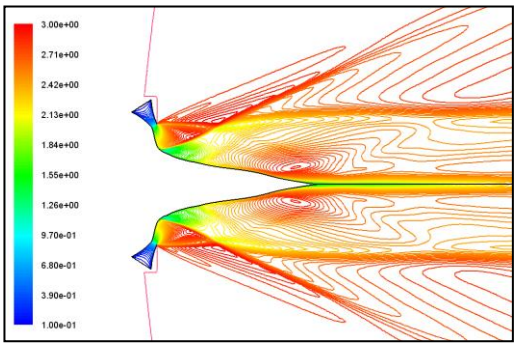

Fig. 6. Mach number contours, shape 1, Pr = 1.

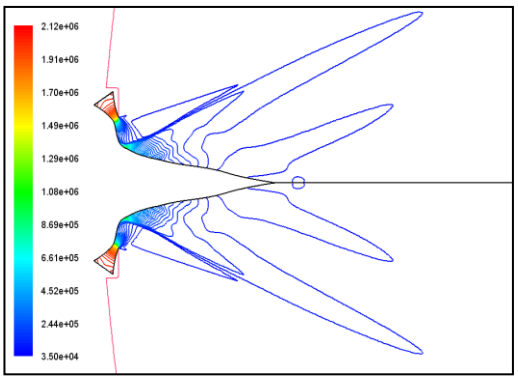

Fig. 7. Pressure contours, shape 1, Pr = 1.

Figs. 8 and 9 illustrate the Mach number and pressure contours for shape 2. No shock wave is observed in this shape due to smooth change of the plug curvature.

The Mach number and pressure contours of shape 3 are demonstrated in Figs. 10 and 11. The flow pattern is very similar to that of shape 2. However, the expansion waves are weaker in this case due to decrease in the curvature compared to shape 2. Expansion waves of shape 3 persist near the end of the plug.

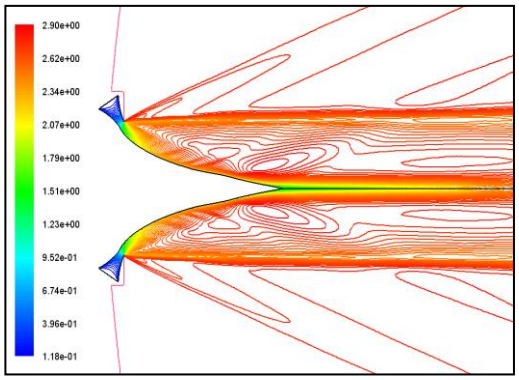

Fig. 8. Mach number contours, shape 2, Pr = 1.

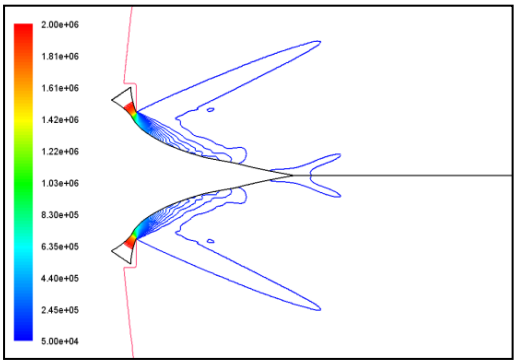

Fig. 9. Pressure contours, shape 2, Pr = 1.

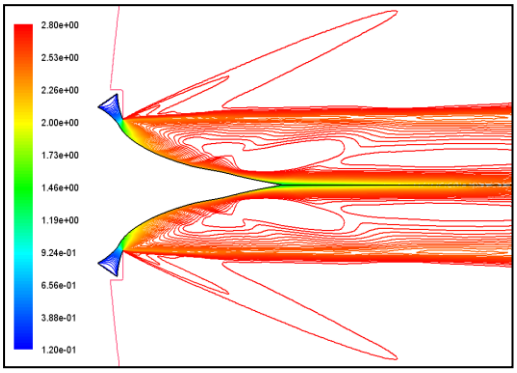

Fig. 10. Mach number contours, shape 3, Pr = 1.

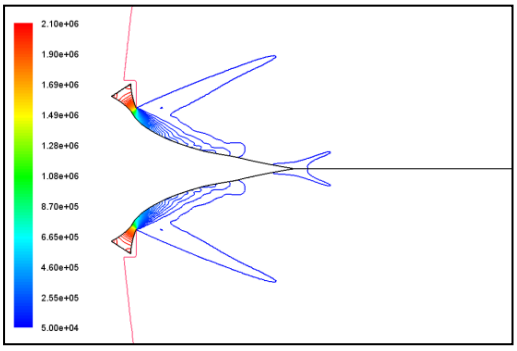

Fig. 11. Pressure contours, shape 3, Pr = 1.

In shape 4, a shock wave happens slightly after the nozzle throat due to a sudden change in the curvature. Mach number and pressure contours of this shape are shown in Figs. 12 and 13. The expansion waves followed by the shock wave are continued up to the end of the plug, as it will be seen later, and provides more thrust over the spike. To reduce the shock wave strength, the gradient of the leading part of the spike decreases in shape 5. Figs. 14 and 15 show the Mach number and pressure contours of shape 5. The figures show the reduction in the second shock wave along the spike. Therefore, the gradient of the spike decreases more in shape 6.

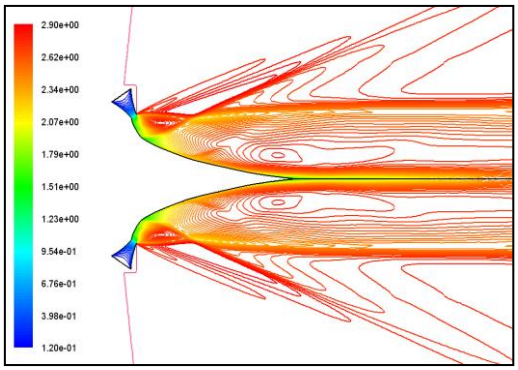

Fig. 12. Mach number contours, shape 4, Pr = 1.

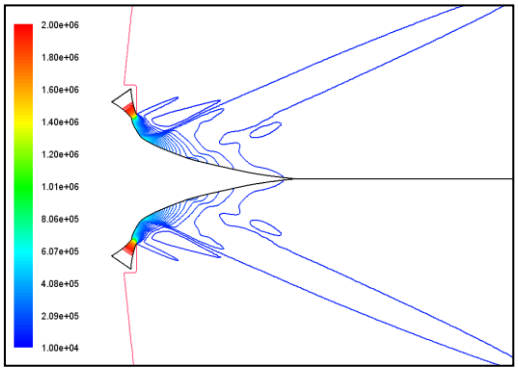

Fig. 13. Pressure contours, shape 4, Pr = 1.

The thrust force of the aerospike nozzle with different plugs is briefly listed in Table 2. The three components given in this table are the terms of the thrust in Eq. (5). The Mach number and pressure contours of this shape are shown in Figs. 16 and 17. The shock wave is disappeared in this case. However, the expansion waves are ended before the end of the plug, as it is seen in the results, in the reduction of the thrust force produced over the spike.

Table 2. Thrust force for different spike shapes*, PR=1.

Case #	T1	T2	T3	Total thrust
Shape 1	1015.6	915.18	899.16	2830.01
Shape 2	1003.5	791.62	2439.1	4234.25
Shape 3	918.73	1163.7	1914.7	3997.29
Shape 4	1016.9	906.80	2361.1	4284.94
Shape 5	1013.6	915.46	2410.9	4340.09
Shape 6	997.49	948.14	2358.1	4303.75

∗The thrust forces are all measured in N.

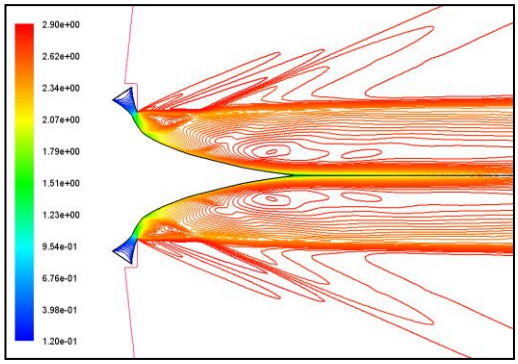

Fig. 14. Mach number contours, shape 5, Pr = 1.

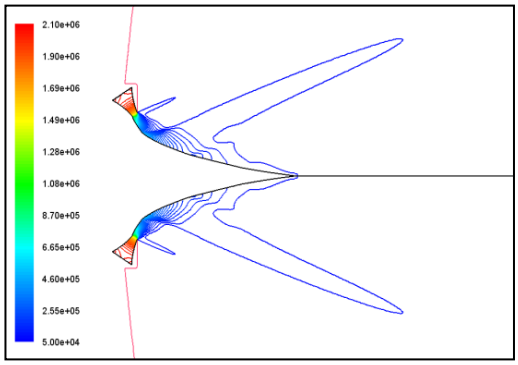

Fig. 15. Pressure contours, shape 5, Pr = 1.

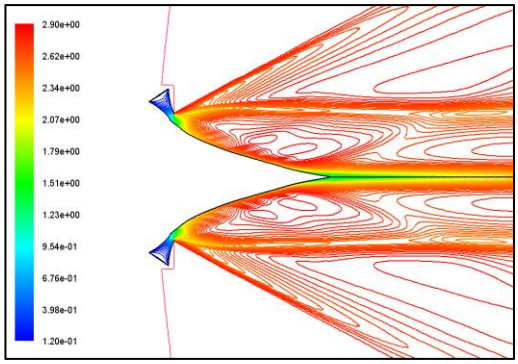

Fig. 16. Mach number contours, shape 6, Pr = 1.

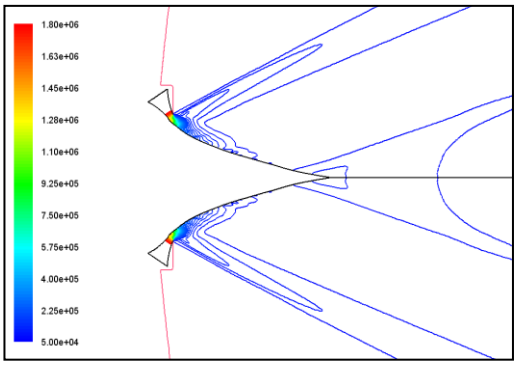

Fig. 17. Pressure contours, shape 6, Pr=1.

The last term (T_3) indicates the thrust over the spike part of the nozzle. The maximum spike thrust force and also the maximum total thrust belong to shape 5. As mentioned previously, the thrust over the spike of shape 6, compared to shape 5, is remarkably reduced. The minimum thrust is related to case 3 which has the steepest gradient.

5.2. Over expansion condition

In this case, it is generally expected that the shock and expansion waves occur to adjust the pressure over the spike to the ambient pressure. However, the strength and number of expansion and compression waves depend on the spike shape. The Mach number and pressure contours of shape 1 are shown in Figs. 18 and 19, respectively. A strong shock wave stands at the beginning part of the spike. This shock wave is followed by weak expansion and compression waves until reaches the ambient pressure.

In shape 2, expansion and compression waves occur over the spike (Figs. 20 and 21) but in comparison with the previous shape, the increase in the Mach number over a large area over the spike is followed by a rather weak shock wave at the end. Due to its curvature right after the throat, the compression waves over spike 3 are much stronger than shape 2.

The Mach number contours of this shape are presented in Fig. 22. Besides, Fig. 23 shows that small expansion waves happen at the end of the plug.

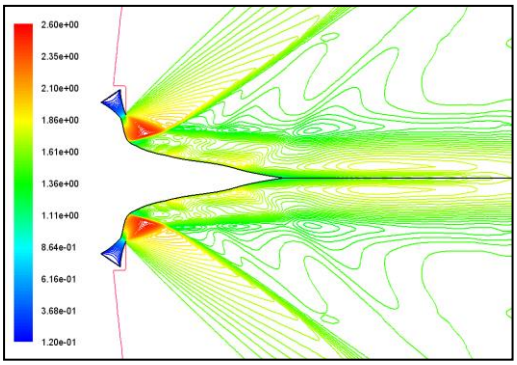

Fig. 18. Mach number contours, shape 1, PR=4.

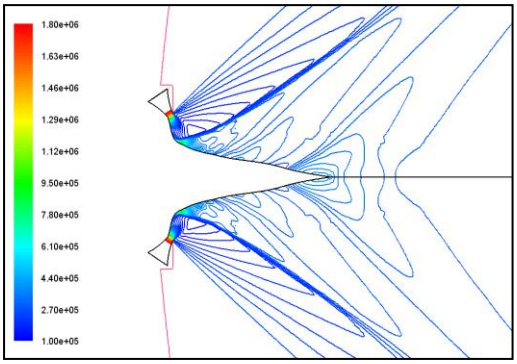

Fig. 19. Pressure contours, shape 1, PR=4.

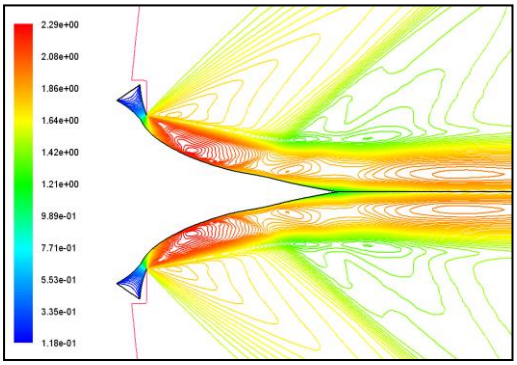

Fig. 20. Mach number contours, shape 2, PR =4.

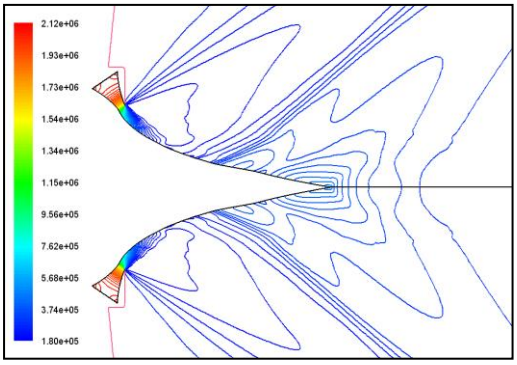

Fig. 21. Pressure contours, shape 2, PR =4.

Figs. 24 to 27 present the contours for shape 4 and shape 5. The flow features of these cases are similar to that of shape one except that the shock wave is comparably weaker than shape 1. The expansion waves extend a small distance over the plug in plugs 4 and 5. The curvature changes in shape 6 are smoother than shape 5. Both compression and expansion waves are weak in this case. Figs. 28 and 29 represent the Mach and pressure contours of shape 6.

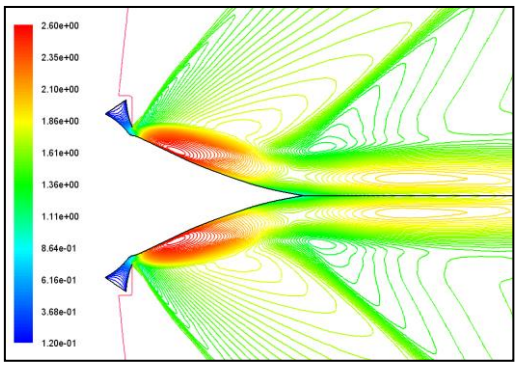

Fig. 22. Mach number contours, shape 3, PR =4.

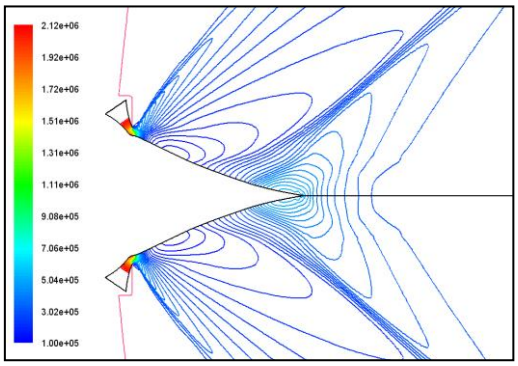

Fig. 23. Pressure contours, shape 3, PR =4.

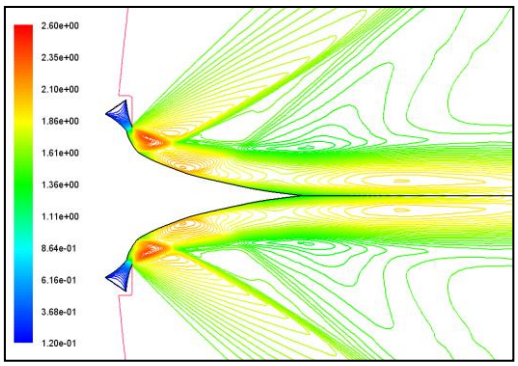

Fig. 24. Mach number contours, shape 4, PR =4.

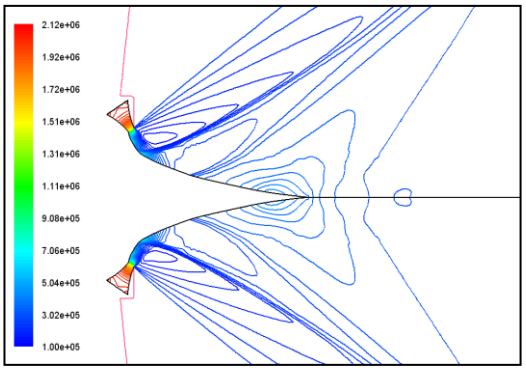

Fig. 25. Pressure contours, shape 4, PR =4.

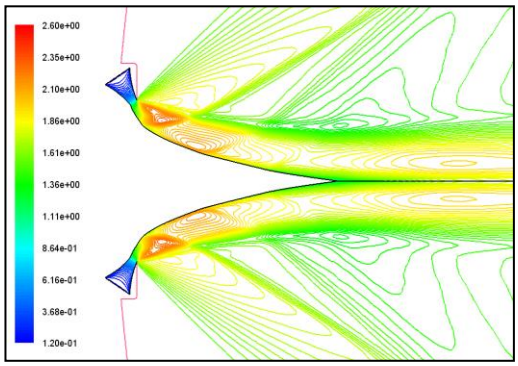

Fig. 26. Mach number contours, shape 5, PR =4.

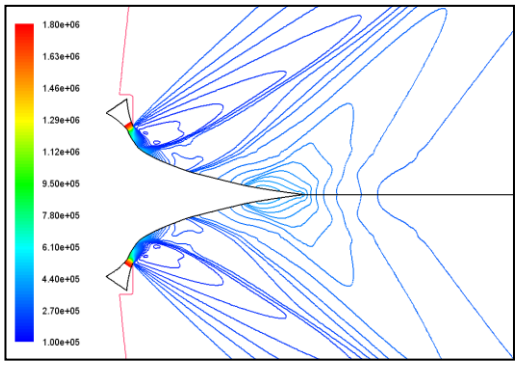

Fig. 27. Pressure contours, shape 5, PR =4.

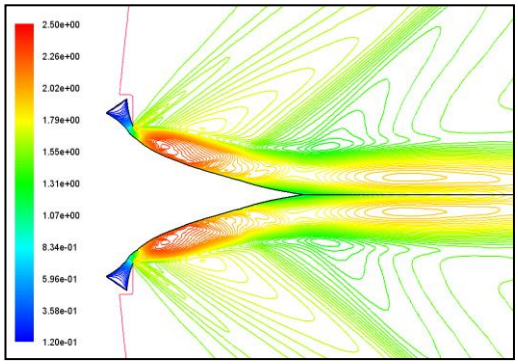

Fig. 28. Mach number contours, shape 6, PR =4.

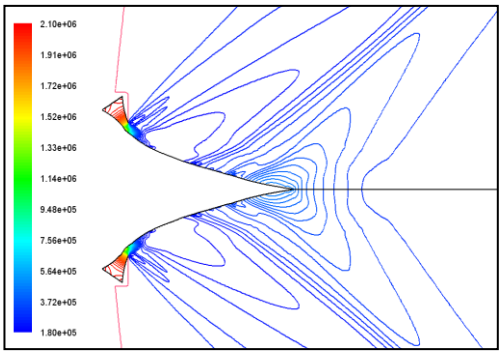

Fig. 29. Pressure contours, shape 6, PR =4.

The thrust forces of the over expansion condition are given in Table 3. The maximum spike thrust force and the total force is related to shape 2.

Table 3. Thrust force for different spike shapes*, PR=4.

Case #	T1	T2	T3	Total thrust
Shape 1	1017.776	767.2883	1086.095	2871.15917
Shape 2	1004.284	795.1601	1449.416	3248.8602
Shape 3	921.5315	1021.241	1081.592	3024.36519
Shape 4	1018.677	761.5346	1316.678	3096.88881
Shape 5	1015.363	770.839	1394.693	3180.89469
Shape 6	1001.265	801.2203	1430.198	3232.68268

*The thrust forces are all measured in N.

5.3. Under expansion condition

Under expansion condition, the throat pressure is more than the ambient pressure, so the flow over the spike continues to expand until achieving the ambient pressure. Figs. 30 and 31 show the Mach number and pressure contours of shape 1. Here the shock wave is much weaker in comparison with Figs. 18 and 19.

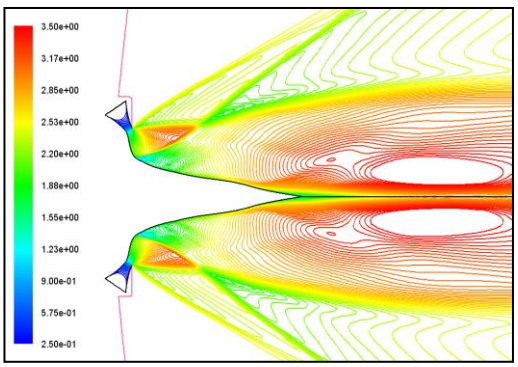

Fig. 30. Mach number contours, shape 1, PR =0.41.

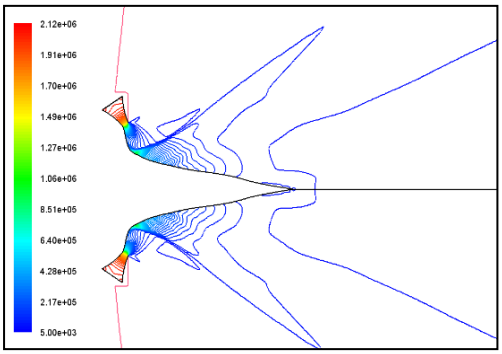

Fig. 31. Pressure contours, shape 1, PR =0.41.

The compression waves approximately extend a large part of the spike. In shape 2, there is no shock wave as expected, and the expansion waves include the entire plug. These are shown in Figs. 32 and 33. Some expansion waves are observed over a small part of the spike 3 in Figs. 34 and 35. The expansion waves are then followed by compression waves. The flow structure in this shape is much more similar to the over-expansion condition due to the configuration of the spike. The compression waves are gradually eliminated in shapes 4, 5 and 6, and the expansion waves cover the entire spike.

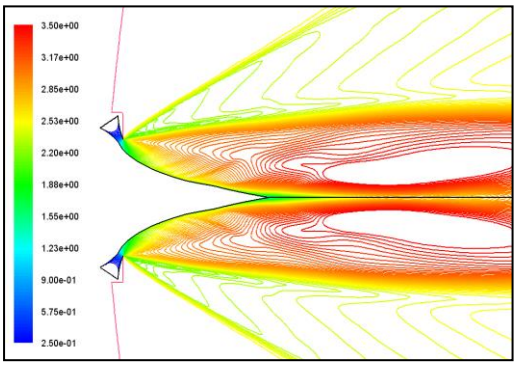

Fig. 32. Mach number contours, shape 2, PR =0.41.

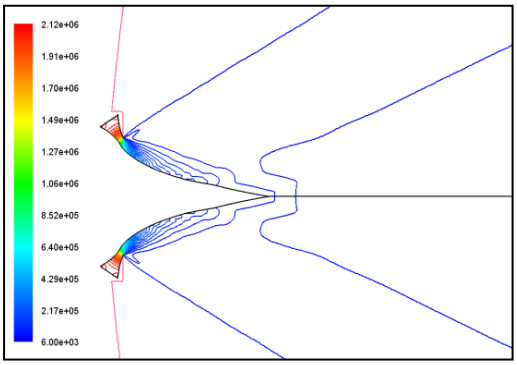

Fig. 33. Pressure contours, shape 2, PR =0.41.

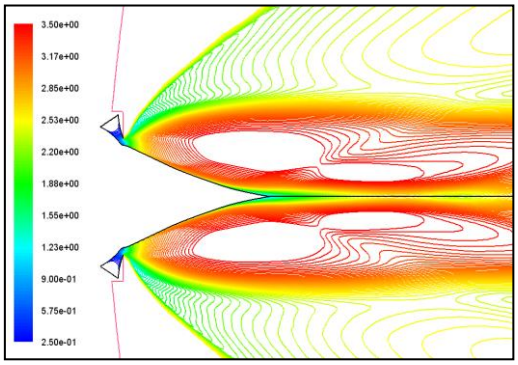

Fig. 34. Mach number contours, shape 3, PR =0.41.

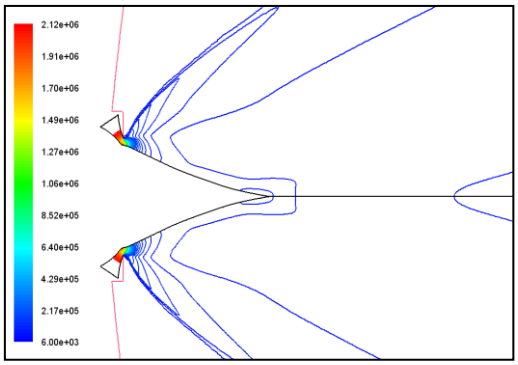

Fig. 35. Pressure contours, shape 3, PR =0.41.

Nevertheless, the Mach number decreases in these cases as well. These are illustratively shown in Figs. 36-41. The computed thrust force components and the total force are shown in Table 4. Again the maximum spike thrust and total thrust force are related to shape 2. To study the performance of different spike configurations, the thrust force is plotted against pressure ratios in Fig. 42 for all aerospike nozzles. Since the thrust force of shape 1 is considerably different with other shapes, it is removed from this figure.

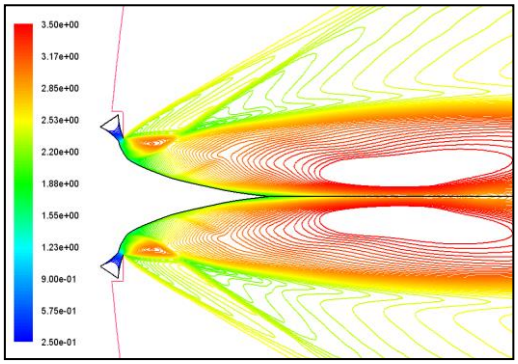

Fig. 36. Mach number contours, shape 4, PR =0.41.

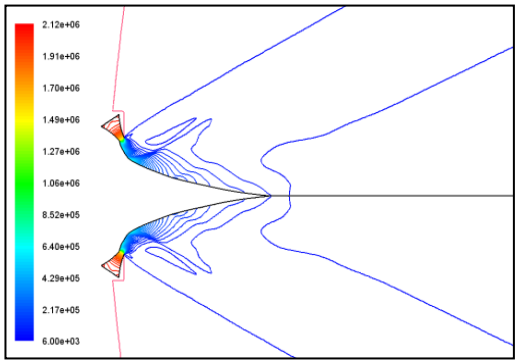

Fig. 37. Pressure contours, shape 4, PR =0.41.

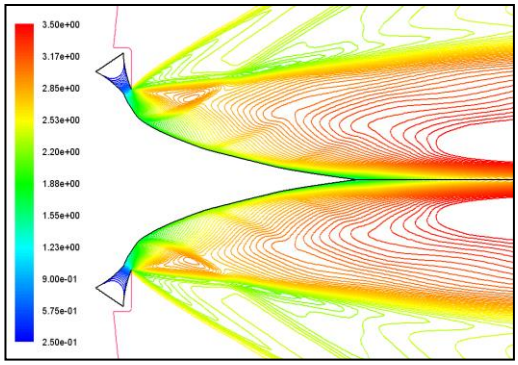

Fig. 38. Mach number contours, shape 5, PR =0.41.

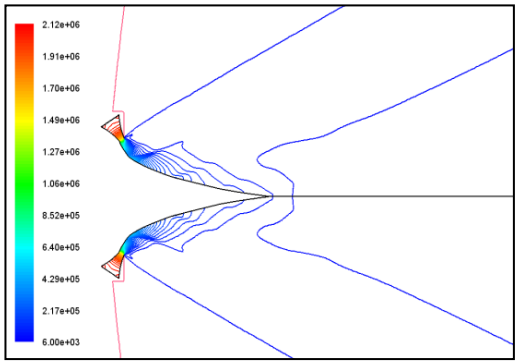

Fig. 39. Pressure contours, shape 5, PR =0.41.

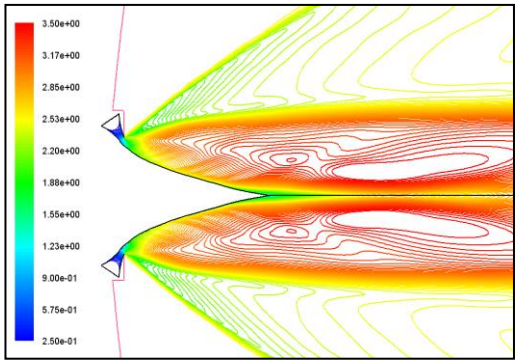

Fig. 40. Mach number contours, shape 6, PR =0.41.

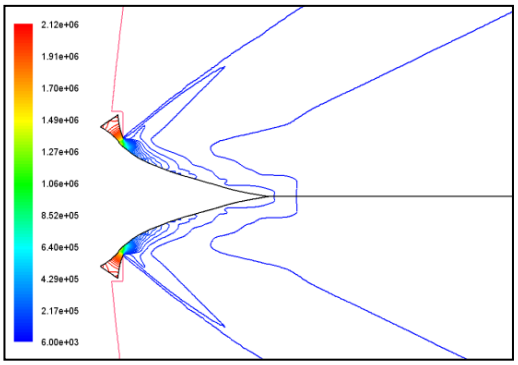

Fig. 41. Pressure contours, shape 6, PR =0.41.

Table 4. Thrust force for different pike shapes*, PR=0.41

Case #	T1	T2	T3	Total thrust
Shape 1	1016.387	942.6952	2386.723	4345.80529
Shape 2	1003.347	969.4337	2677.327	4650.10802
Shape 3	920.4651	1191.557	2142.224	4254.24599
Shape 4	1018.819	937.686	2607.528	4564.03307
Shape 5	1014.182	947.1467	2662.679	4624.00703
Shape 6	1000.366	976.5898	2596.317	4573.27274

*The thrust forces are all measured in N.

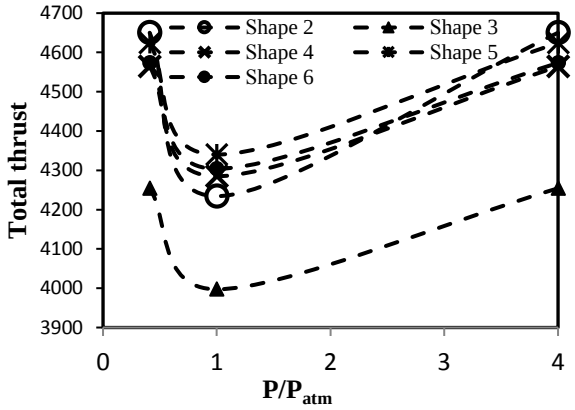

Fig. 42. Thrust force variation versus pressure.

Evidently, shape 3 is the worst case with the minimum thrust force among all conditions. Shapes 2 and 5 have nearly the same thrust force in over and under-expansion condition but in design condition; shape 5 performs better than shape 2. Consequently, according to the thrust force results, aerospike nozzle with plug 5 is more appropriate than other configurations. In the meanwhile, as mentioned in Introduction, a second important parameter in aerospike nozzle design is the temperature increase over the plug that is of special importance.

To consider the thermal effects over the plug, the flow temperature curve over the spike is shown in Figs. 43-45 for design, over-expansion and under-expansion conditions. Almost in all conditions, spike 1 has the most flow temperature over the spike. This is due to the strong shock wave that is formed over the spike. Both spikes 2 and 5 have acceptably small flow temperature. Accordingly, it can be decided that shape 5 is the most appropriate configuration among all generated shapes.

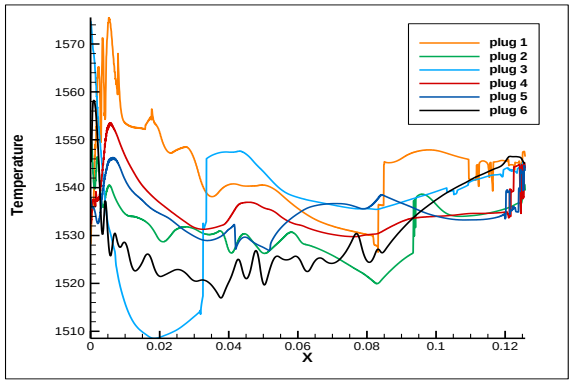

Fig. 43. Temperature distribution over plug, PR 1.

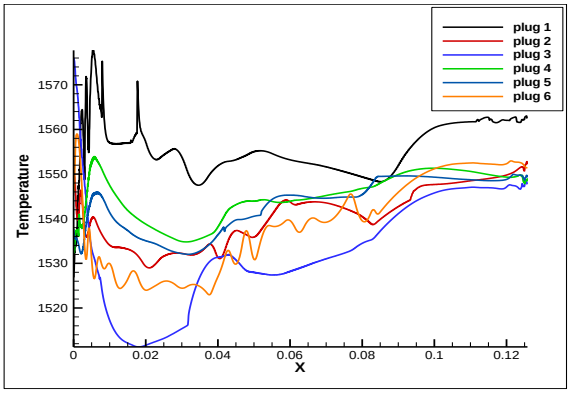

Fig. 44. Temperature distribution over plug, PR=4.

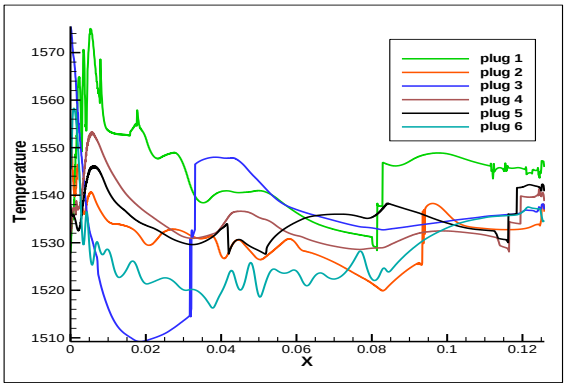

Fig. 45. Temperature distribution over plug, PR =0.41.

6. Conclusions

In the current research, the flow properties of different aerospike nozzle shapes are studied. The flow field is simulated using steady-state, density based Navier-Stokes equations and k-ε turbulence model. Different plug shapes are generated using uniform Cubic B-Spline curve, and their flow properties are studied. The effect of changes in the curvature of the plug in flow phenomena is elaborated in design, under and over- expansion cases. It is shown that increasing the plug slope results in more expansion waves, but if the slope is too sharp, it decreases the length of the plug, and the total thrust decreases accordingly. The thrust force components are calculated for each case, and the best configuration is determined in terms of the maximum thrust generation. Since the temperature rise is a limiting parameter in the aerospike nozzle design, the temperature distribution is calculated along the nozzle for further investigations. According to the results, the best nozzle among the test cases exhibits a relatively lower temperature rise compared to other designs. Total thrust force and the flow temperature are considered as the performance parameters, and the best configuration is determined.

References

[1] J. Hall, "Optimized Dual Expander Aerospike Rocket", Department of the Airforce Air University Airforce Instituite of Technology, US, Ohio, (2011).

[2] T. A. Ladeinde, *Performance Comparison Between a Full-Length and a Truncated Aerospike Nozzle*, Msc thesis Department of Mechanical and Aerospace Engineering, California State University, Long Beach, (2009).

[3] M. Nazarinia, A. Naghib-Lahouti, E. Tolouei, "Design and Numerical Analysis of Aerospike Nozzles with Different Plug Shapes to Compare their Performance with a Conventional Nozzle", *AIAC-11 Eleventh Australian International Aerospace Congress*, Melbourne, Australia,13-17 March, (2005).

[4] E. Besnard, H. Chen, T. Mueller, and J. Garvey, "Design, Manufacturing and Test of a Plug Nozzle Rocket Engine", *Proceedings of the 38th AIAA/ASME/SAE/ASEE Joint Propulsion Conference & Exhibit*, (2002).

[5] E. S. Mcvay, "Design of a Dual-Expander Aerospike Nozzle Rocket Engine", *MSC Thesis, Department of Aerospace Engineering and Mechanics in the Graduate School of the University of Alabama*, (2016).

[6] P. Lemieux, "Development of a Reusable Aerospike Nozzle for Hybrid Rocket Motors", *39th AIAA Fluid Dynamics Conference*, San Antonio, Texas, (2009).

[7] T. Karthikeyan, S. K. Aravindhkumar, J. Arun Kumar, "Design and Analysis of Aerospike Nozzle toImprove Thrust in Hybrid Rocket Engine", *International Journal of Engineering Trends and Techno logy*, Vol. 36, No. 7, (2016).

[8] T. Niimi, H. Mori, K. Okabe, Y. M. Taniguchi, "Analyses of Flow Field Structures Around Linear-Type Aerospike Nozzles Using LIF and PSP", *20th International Congress on Instrumentation in Aerospace Simulation Facilities*, (2003).

[9] T. Wang, "Effect of Fence on Linear Aerospike Plume-Induced Base-Heating Physics", *Journal of Thermo physics and Heat Transfer*, Vol. 14, No. 4, (2000).

[10] T. Zebbiche, Z. Youbi, "Supersonic Two-Dimensional Plug Nozzle Conception at High Temperature" , *Emirates Journal for Engineering Research*, Vol. 11, (2006).

[11] S. B. Verma, "Performance Characteristics of Annular Conical Aerospike Nozzle with Free stream Effect", *Journal of Propulsion and Power*, Vol. 26, No. 3, (2009).

[12] A. Naghib-Lahouti, E. Tolouei, "Investigation of the Effect of Base Bleed on Thrust Performance of a Truncated Aaerospike Nozzle in Off-Design Conditions", *European Conference on Computational Fluid Dynamics*, ECCOMAS CFD, Delft, Netherlands, (2006).

[13] A. Zilic, D. L. Hitt, and A. A. Alexeenko, "Numerical Simulations of Supersonic

Flow in a Liear Aerospike Micronozzle", *37th AIAA Fluid Dynamics Conference and Exhibit*, 25-28 Jun, Miami, FL, (2007).

[14] T. W. Simpson, F. Mistree, "Multidisciplinary Approach to Linear Aerospike Nozzle Optimization", *AIAA journal*, Vol. 39, No. 12, (2001).

[15] A. N. Kraiko, N. I. Tillyayeva, "Contouring Spike Nozzles and Determining the Optimal Direction of Their Primary Flows", *Journal of Fluid Dynamics*,Vol. 42, No. 2, (2007).

[16] O. Bozic, D. Porrmann, "Estimation of Flow Field Properties and Thrust Performances of Axisymmetric Plug-Nozzles using CFD Simulations", *Turbulence, Heat and Mass Transfer 6*, 14-18 September, Rome, Italy, (2009).

[17] M. Imran, "Introduction to Aerospike and its Aerodynamic Features", *ınternational Journal of Scientific and Research Publications*, Vol. 6, No. 5, (2016).

How to cite this paper:

A. Shahrokhi and S. Noori, "Favorable plug shape of an aerospike nozzle in design, over and under expansion conditions" *Journal of Computational and Applied Research in Mechanical Engineering*, Vol. 8, No. 1, pp. 1-14, (2018).

DOI: 10.22061/jcarme.2017.2162.1243

URL: http://jcarme.sru.ac.ir/?_action=showPDF&article=775